J Mol Model (2015) 21:55
DOI 10.1007/s00894-015-2604-6

ORIGINAL PAPER

Enantiomeric discrimination of chiral organic salts by chiral aza-15-crown-5 ether with C_1 symmetry: experimental and theoretical approaches

Safak Özhan Kocakaya · Yılmaz Turgut · Necmettin Pirinççioglu

Received: 26 September 2014 / Accepted: 1 February 2015

Abstract The work involves an experimental (^{1}H NMR) and theoretical (MD, MM-PBSA and DFT) investigation of the molecular recognition and discrimination properties of a chiral aza-15-crown-5 against methyl esters of alanine, phenylalanine and valine hydrochloride salts. The results indicate that the receptor binds enantiomers with moderate binding constants (88–1,389 M^{-1}), with phenylalanine being more discriminated. The difference in experimental binding free energies ($\Delta G^R - \Delta G^S$) for alanine, phenylalanine and valine enantiomers were calculated as −0.36, −1.58 and 0.80 kcal mol^{-1}, respectively. The differences in theoretical binding energies were calculated by MM-PBSA ($\Delta E^R_{PB} - \Delta E^S_{PB}$=) as −0.30, −1.45 and 0.88, by B3LYP/6-31+G(d) as −1.17, −0.84 and 0.74 and by M06-2X/6-31+G(d) as −1.40, −3.26 and 1.66 kcal mol^{-1}. The data obtained give valuable information regarding the molecular recognition mode of the organoammonium complexes of chiral aza-crown ether with C_1 symmetry, which may be relevant to biological systems.

Keywords Enantiomeric discrimination · Chiral aza-crown ether · Molecular recognition · Amino acid ester salt · ^{1}H NMR titration · Computational calculation · Molecular dynamics · MM-PBSA · DFT

Electronic supplementary material The online version of this article (doi:10.1007/s00894-015-2604-6) contains supplementary material, which is available to authorized users.

S. Ö. Kocakaya · Y. Turgut · N. Pirinççioglu (✉)
Department of Chemistry, Faculty of Science, University of Dicle, Diyarbakir 21280, Turkey
e-mail: pirincn@dicle.edu.tr

Introduction

Molecular recognition, including chiral discrimination, is one of the greatest challenges presented to science by nature. Indeed, chirality itself still represents a puzzle to science [1, 2]. Therefore, studying this phenomenon remains an outstanding subject of current research. The significance of studies on chiral discrimination and their application has been repeatedly honored, for example with Nobel prizes being awarded to W. S. Knowles, R. Noyori, and K. B. Sharpless in 2001 [3–5]. However, given the challenges of studying the main forces behind this process in nature, there are still many questions to be answered in this field. Scientists employ models to gain insight into this subject [6–10]. Chiral recognition is one of the most important issues in the field and many models have been developed [11–15]. Crown ethers, synthesized by Cram et al. [16], were the first enantioselective receptors identified for primary organoammonium salts. Since then, a great number of artificial chiral receptors have been developed and studied [17–36]. Presently, crown ether derivatives **1**–**4** showing C_1 and C_2 symmetry act as receptors for primary organoammonium salts (Scheme 1) [37–39]. The current macrocycle **5** with C_1 symmetry also forms stable complexes with organoammonium salts [39].

However, despite significant advances in modeling techniques and the comparative simplicity of host-guest systems, there is still a need to understand molecular recognition at the atomic level and to interpret experimental data using computational tools. Ultimately, such studies will aid the design of new hosts for targeted molecular guests. Molecular dynamics (MD) is one of the methods currently used in the understanding of molecular recognition processes occurring in organisms at the atomic level and, consequently, free energy calculations have became a powerful tool in estimating the quantitative degree of

Published online: 21 February 2015

Scheme 1 Crown ether derivatives**1**–**4** showing C_1 and C_2 symmetry act as receptors for primary organoammonium salts. Macrocycle **5** with C_1 symmetry also forms stable complexes with organoammonium salts

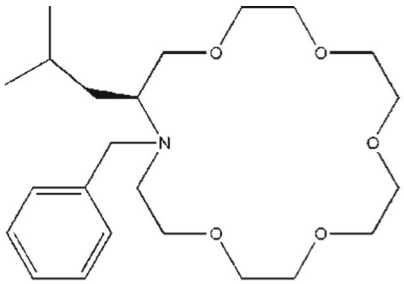

1

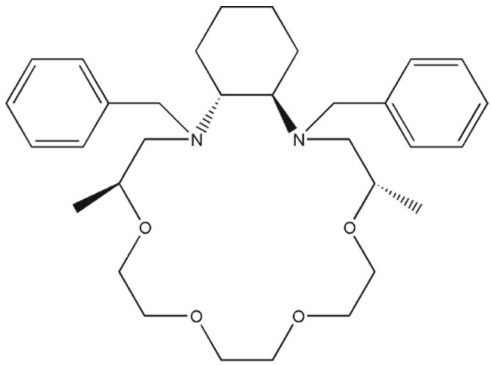

2

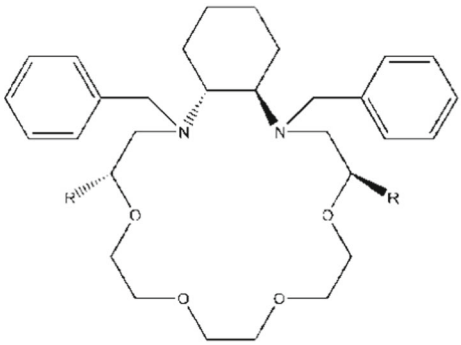

3 (R=Ph, CH_2OPh)

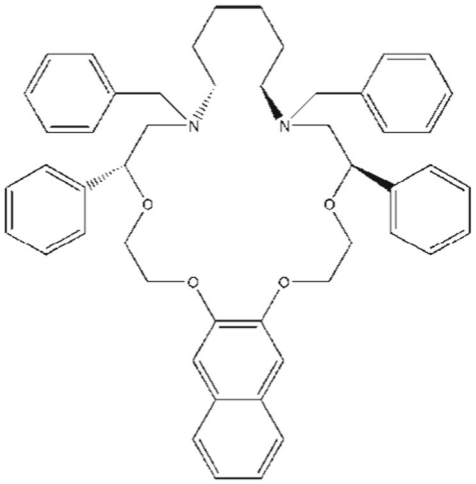

4

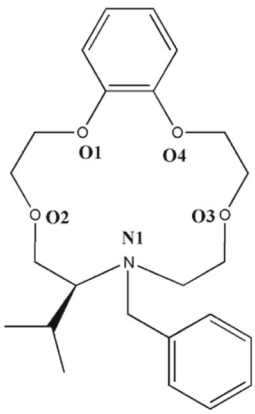

5

molecular interactions in host-guest chemistry. The method has been developed for biological systems but has also been used in supramolecular systems of organic structures [40, 41], even in predicting chiral discrimination [42, 43]. The MM-PB(GB)SA method [44], which has been applied successfully to estimate the binding free energies of different biological systems [45–56], is one of the most valuable methods.

The present study investigated the complexation and discrimination ability of chiral crown ether **5** with C_1 symmetry with methyl esters of alanine, phenylalanine and valine hydrochloride salts. A ^{1}H NMR titration technique was used to calculate the binding constants and thus the enantiomeric discrimination of this receptor against the enantiomeric pairs since this is known as one of the most effective tools in studying host-guest supramolecular chemistry [57, 58]. MD

computation was also employed to predict the mode of complexation as well as to estimate the binding energy of the complexes of the receptor with the enantiomer salts using MM-PBSA. Quantum mechanical computation was also applied to calculate the binding free energies of the complexes by the density functional theory (DFT) method at B3LYP/6-13+g(d) and M062X/6-31+g(d) levels of theory. It was interesting to note that theoretical data produced results comparable with those obtained from experimental observations.

Materials and methods

All substrates and deuterated NMR solvents were obtained from commercial suppliers and used without further purification. The synthesis of the host was reported previously [39]. Spectra were recorded on BRUKER 400 MHz NMR spectrometer at 300 K at ambient probe temperature and calibrated using tetramethylsilane (TMS) as an internal reference. Graphpad PRISM software 4 version (GraphPad Software, La Jolla, CA, http://www.graphpad.com) was used for non-linear curve fitting to obtain binding constants.

Experimental methods

NMR titration

A range of stock solution of the ligands (0–10^{-4} M) containing a constant amount of the receptor (10^{-3} M) in choloroform-d1 was prepared and their ^{1}H NMR spectra (16 scans, sweep width 20.7 ppm, digital resolution 18, pulse angle 30°, delay time 1 s) were collected at 300 K at ambient probe temperature and calibrated using TMS as an internal reference. The changes in chemical shift of the methyl group of the isopropyl moeity in the host against the concentration of guests were fitted to Eq. 4 derived from Eqs. 1–3 and thus the non-linear curve fitting the binding constants for each enantiomer was calculated.

$$R + L \underset{k_{-1}}{\overset{k_1}{\rightleftharpoons}} R.L \tag{1}$$

$$K_{diss} = k_1/k_{-1} = [R][L]/[R.L] \tag{2}$$

$$[L] = [L]_{free} + [L]_{complex} \tag{3}$$

$$\delta_{obs} = \left(\delta_0 K_{diss} + \delta_{max}[L]_{tot}\right)/\left(K_{diss} + [L]_{tot}\right) \tag{4}$$

where δ_{obs} is the observed chemical shift in ^{1}H NMR of any specific hydrogen in a receptor or ligand upon complexation, δ_0 is the corresponding chemical shift in the absence of the added ligand, while δ_{max} is the maximum chemical shift achieved in the same ^{1}H NMR signal. $[L]_{tot}$ is the total concentration of ligand and K_{diss} is the dissociation constant between receptor and ligand.

Computational methods

Molecular dynamics simulations

MD calculations were carried out in a Linux-Cluster system. All simulations were run by using the AMBER (version 9.0) suite of programs [59]. The host and ligands were designed by GaussView 3.09 and optimized with Gaussian 03 [60] using the semi-empirical AM1 method [61]. AM1-Bcc (Austian model with Bond and charge correction) [62, 63] atomic partial charges for the receptor were determined by the antechamber module of the AMBER (v9) package. The charges and parameters for amino acid esters were obtained from the ff99SB library [64]. The general AMBER force field (GAFF) [65] was used for the receptor.

The receptor molecule was minimized with a total of 5,000 steps, 2,500 of steepest descent followed by 2,500 of conjugate gradient (maxcyc-ncyc), using a nonbonded cutoff of 999 Å and a generalized Born solvent model (igb=0). The system was then heated from 0 to 700 K in 14 steps for a period of 350 ps and further simulated at 700 K for a period of 20,000 ps (igb=0). A cluster analysis was performed with 67 intervals out of 20,000 frames to obtain a conformer with a larger population to represent the lower energy conformer. The complexes were prepared by locating each ligand on the surface of the crown ring so that maximum contact points through hydrogen bonds between ammonium and crown donors were achieved. The complexes were minimized with a total of 5,000 steps, 2,500 of steepest descent, followed by 2,500 of conjugate gradient, using a nonbonded cutoff of 999 Å and a generalized Born solvent model (igb=0). The system was then heated from 0 to 700 K in 14 steps for a period of 350 ps and further simulated at 700 K for a period of 20,000 ps (igb=0). A cluster analysis was performed with 67 intervals out of 20,000 frames and the coordinates of the structure with the largest population was recorded. This conformer was minimized followed by cooling from 700 to 300 K in eight steps for a period 200 ps and further computed at 300 K for a period of 20,000 ps. MD coordinates were recorded with 1.0 ps intervals. A cluster analysis was used to obtain the conformer with the largest population for each complex.

The ptraj module of AMBER was used to analyze energy changes and root-mean-square displacement (RMSD) for the hosts and complexes as well as the average bond distances (contact point analysis) between atoms in the receptor and in the ligands. Chimera (UCSF) [66] was employed to display 3D structures and cluster analyses and the programme

GraphPad Pris 4 pocket was used in generating energy and RMSD graphics.

Molecular mechanics-Poisson-Boltzmann surface area

The molecular mechanics-Poisson-Boltzmann surface area (MM-PBSA) module of AMBER (v11) was applied to compute the binding free energy ($\Delta G_{\text{binding}}$) of each complex [67, 68]. For each complex, a total number of 200 snapshots were extracted from the last 10 ns of the complex trajectories. In the MM-PBSA, the binding free energy of a ligand (L) to a receptor (R) to form the complex (RL) is described by Eq. 5.

$$\Delta G_{binding} = G(RL) - G(L) - G(R) \tag{5}$$

The free energies of individual species in Eq. 5 are given by Eq.6.

$$G(X) = H(X) - TS(X),\ and\ hence G(X) = U(X) + PV(X) - TS(X) \tag{6}$$

The effects on binding free energy due to small volume changes on conversion from a canonical to an isothermal-isobaric ensemble are neglected and thus Eq. 6 takes the form:

$$G(X) = E_{MM}(X) + G_{solv}(X) - TS(X) \tag{7}$$

Where $U(X) \approx E_{\text{MM}}(\text{X}) + G_{\text{solv}}(\text{X})$ and the E_{MM} term refers to the total molecular mechanics energy of molecular system X in the gas phase, which is the sum of the bonded (internal), and non-bonded electrostatic and van der Waals energies as defined by Eq. 8. G_{solv} corresponds to a correction term (solvation free energy), meaning that X is surrounded by solvent, and S is the entropy of X.

$$E_{\text{MM}} = E_{\text{bonded}} + E_{\text{elec}} + E_{\text{vdw}} \tag{8}$$

Changes (Δ) in the individual terms (ΔE_{MM}, ΔG_{solv}, $-\text{T}\Delta\text{S}$) of Eq. 7 between the unbound states and the bound (complex) state were calculated, and contributed to the binding free energies according to Eq. 5.

These energy contributions were calculated from the atomic coordinates of the receptor, ligand and complex using the (gas phase) molecular mechanics energy function (force field) using the force field of Cornell et al. [69] with no cutoff. The solvation free energy term G_{solv} involves both polar and non-polar contributions where the former contributions are accounted for by the generalized Born, Poisson, or Poisson-Boltzmann model, and the latter are assumed to be proportional to the solvent-accessible surface area (SASA).

$$G_{solv} = G_{PB(GB)} + G_{SASA} \tag{9}$$

Theoretically, most implicit solvent models break up the solvation process into three sequential steps [70]: (1) creation of a cavity in solution to accommodate the receptor; (2) switching on dispersion interactions between the biomolecule and surrounding medium, while all atomic charges are set to zero; and (3) switching on the biomolecular charges. The first two steps are normally assumed to be proportional to the SASA of the receptor and they (1 and 2) stand for the non-polar contributions (G_{SASA}) to G_{solv} in Eq. 9. The last step (3) computes the contribution to solvation free energy due to the charge/electrostatic interactions of the solute with the surrounding solvent, namely the polar contributions ($G_{\text{PB(GB)}}$) to G_{solv} in Eq. 9. The values for the two parameters (γ and β) depend on the method and solvation model (PBSA or GBSA) employed.

$$G_{nonpolar} = \gamma SASA + \beta \tag{10}$$

where γ is the surface tension proportionality constant (the value is 0.00542 kcal mol^{-1} Å^{-2}). The free energy of nonpolar solvation for a point solute (β) was set to 0.92 kcal mol^{-1}.

In continuum-electrostatics models such as PB and GB, the solute is considered as a low-dielectric cavity surrounded in a high dielectric medium where the solute charges are centered on the individual atoms. The resulting solvation free energy of a molecule X is expressed as [71]:

$$G_{PB(\text{GB})} = \frac{1}{2}\sum_{I,j\in X} q_I q_j g_{Ij}^{\text{PB(GB)}} \tag{11}$$

where the summation is over all the atomic charges $\{q_{\text{I}}\}$. The quantity $g_{\text{ij}}^{\text{PB(GB)}}$ is estimated using the PB model by numerical solution of the Poisson or Poisson-Boltzmann equation (depending on the existence of salt), or using the GB model by an analytical expression with the functional form [71, 72].

$$g_{\text{Ij}}^{\text{GB}} = \left(\frac{1}{\varepsilon} - 1\right)\left[r_{Ij}^{n} B_{Ij} \exp\left(-\frac{r_{Ij}^{n}}{\text{AB}_{Ij}}\right)\right]^{-1/n} \tag{12}$$

The parameters B_{ij} depend on the position (distance from the solute-solvent dielectric boundary) of atoms *I* and *j*, and the shape of the entire biomolecule; ε is the solvent dielectric constant, and r_{ij} is the distance between *I* and *j*. The constants n and A were set to n=2 and A=4 in the original formulation described by Still and coworkers [72]. The dielectric boundary was defined using a 1.4-Å probe on the atomic surface. The

values of the interior dielectric constant and the exterior dielectric constant were set to 1 and 80, respectively.

During conformational searching and the evaluation of configuration integrals, the electrostatic free energy (W_{elec}) was computed with a simplified but fast generalized Born model [72]. The electrostatic solvation energy of each energy-well was then corrected toward a more accurate but time-consuming finite-difference solution of the Poisson equation. The dielectric cavity radius of each atom was set to the mean of the solvent probe radius 1.4 Å for water and the atom's van der Waals radius, and the dielectric boundary between the molecule and the solvent was the solvent-accessible molecular surface. The solvation calculations use a water dielectric constant of 80. The method produces the final estimated binding free energy using both Poisson-Boltzmann and Generalized Born solvation models.

Classical statistical thermodynamics [73] was applied to calculate entropy contributions arising from changes in the degrees of freedom (translational, rotational, and vibrational) of the solute molecules. The normal mode analysis (NMODE) was used to obtain contributions to vibrational entropy [74]. After minimization of each snapshot in the gas phase using the conjugate gradient method with a distancedependent dielectric of 4*r* (with *r* being the distance between two atoms) until the root-mean-square of the elements of the gradient vector was less than 10^{-4} kcal mol^{-1} Å^{-1}, the computation of frequencies of the vibrational modes were carried at 300 K for these minimized structures, including all snapshot atoms and using a harmonic approximation of the energies.

Quantum mechanical calculations

The structure with the highest population for each complex extracted from MD simulations was used for quantum chemical calculations. The calculations were first performed with PM6 [75] and then with B3LYP [76–79] or M062X [80–83] with 6-31+g(d) basis sets without any restriction using Gaussian 09 [84] on Linux with quadro intel process. The calculations using B3LYP/6-31+g(3d) were employed for complexes of the receptor with phenylalanine enantiomers. Calculations at the same levels were also performed in chloroform with the polarizable continuum model (PCM) using the default SCRF method. The discrimination of enantiomer pairs by the receptor was calculated from Eq. 13.

$$\Delta E = (E_R - E_S) \times 627.5 \quad (13)$$

where E_R and E_S are the energy of the complex of each enantiomer in Hartree and 1 Hartree = 627.5 kcal mol^{-1}.

Results and discussion

NMR titration

The standard titration of receptor **5** by methyl esters of (*R*/*S*)-alanine, phenylalanine and valine hydrochloride salts demonstrated complex formation between receptor and ligand. Nine samples were prepared with different receptor/ligand ratios for each ligand, as indicated in the Materials and methods and their NMR spectra were recorded. The data showed that receptor **5** forms 1:1 complexes with the ligands as proved by Job's plots (Fig. 1). A graphical representation of the dependency of ^{1}H NMR shifts on the salt added is represented in Fig. 2 for the enantiomers of alanine and valine ester salts. The data produced a non-linear curve (Fig. 3), which was fitted to Eq. 4 to calculate the dissociation constants for each enantiomer as listed in Table 1. The results show that the receptor forms complexes with methyl ester salts of amino acids with a moderate stability (282–1,515 M^{-1}). The binding constants are smaller than previously reported [37] for the same receptor with organic ammonium salts. This difference in the binding energies of amino acid ester and organoammonium salts may be attributed to the counter ion effect of perchloride and chloride, where the latter has better competing ability with the donors of the receptor compared to the former. However, the difference for the same ligands with different receptors **1**–**4** [37, 38] may be ascribed to the difference in the size of the crown rings, as it is known that a crown with six donors forms better complexes with ammonium salts compared to those with 5 donors [7, 11].

The results also show that the receptor binds preferentially *R*-enantiomers of alanine and phenylalanine salts but *S* enantiomer of valine (Table 1). The results also demonstrate a better capacity to discriminate between the enantiomers of phenylalanine and valine salts compared to those of alanine (Table 1). The enantiomeric discrimination (ED) of the receptor against the enantiomer pairs of methyl ester salts of alanine, phenylalanine and valine was calculated as 65, 83.1 and 79.4, respectively, which correspond to enantiomeric discrimination factors (EDF) of 30.0, 66.2 and 58.8, respectively. ED values were obtained from the ratio of binding constants of enantiomers (*S*/*R*) by assuming *R*+*S*=100. A model may be sketched to rationalize the mode of recognition between receptor and ligand that explains the ED (Fig. 4). The model postulates that the methyl and benzyl groups in alanine and phenylalanine enantiomers with *R* configuration have a more favorable conformational orientation to interact with the benzyl group in the receptor compared to enantiomers with *S* configuration. In contrast, the enantiomer of valine with *S* configuration is preferred to form a more stable complex with the receptor. In this case, it is likely that the isopropyl group in valine with the *S* configuration has a more favorable interaction with the benzene unit in the crown ring.

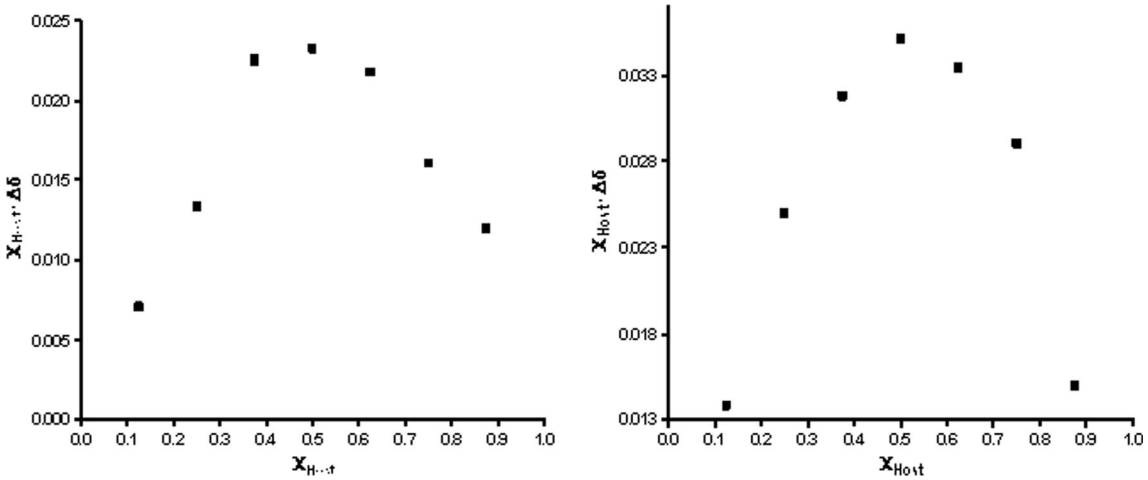

Fig. 1 Job's diagrams for the complex of receptor **5** with methyl esters of *R*-alanine salt (*right*) and *R*-valine (*left*)

Molecular dynamics

MD calculations were performed to understand the mode of the complex formed between the receptor and the ligands and thus the driving forces behind ED at the atomic level. Starting with the correct conformation of the receptor is a crucial step in MD calculations in this type of complex. In this study, the receptor was computed over a period of 20 ns at 700 K, a conformer with a higher population was subsequently cooled down back to 300 K for a period of 20 ns, thereby obtaining the conformer with the highest population from the cluster analysis as shown in Fig. 5a. This conformer indicates that the crown ring remains relatively static and the benzyl group and benzene ring flap during the MD simulation and that the

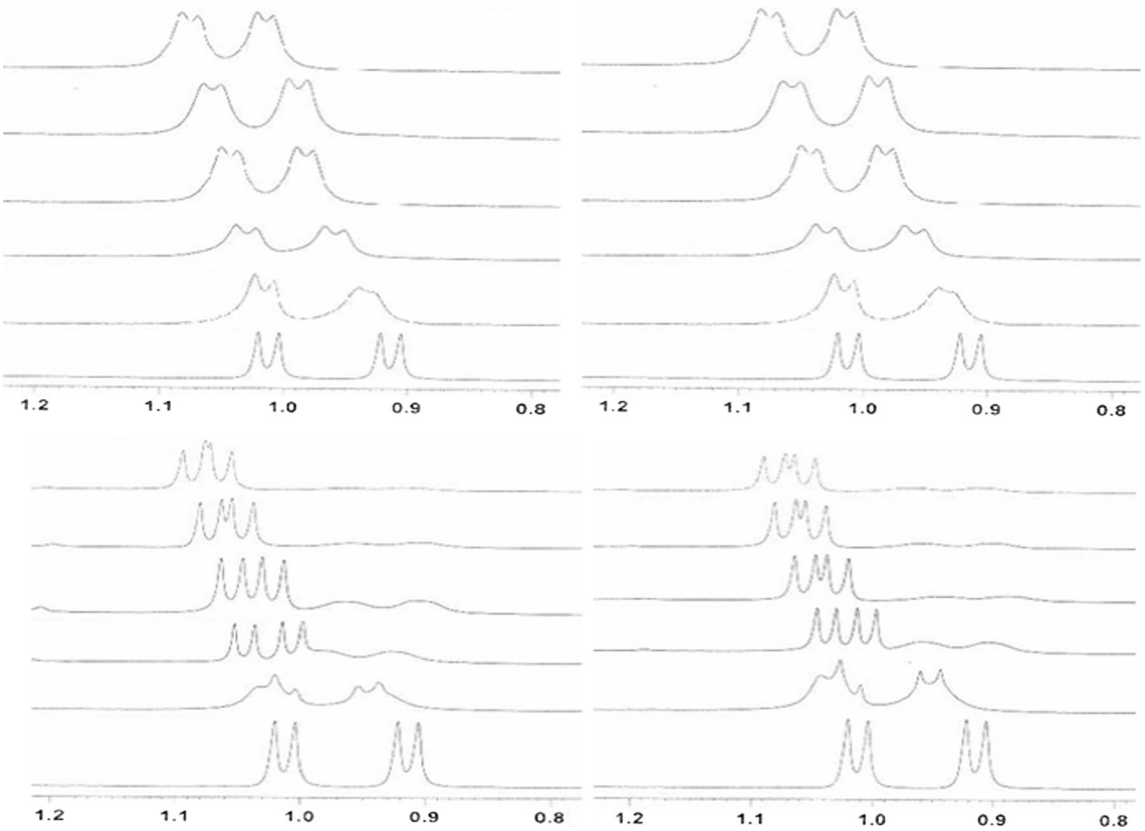

Fig. 2 Dependence on the concentration of the guests of ^{1}H NMR chemical shifts of methyl groups of isopropyl in receptor **5**. Upper line: *Left R*-alanine methyl ester salt, *right S*-alanine methyl ester salt. Lower line: *Left R*-valine methyl ester salt, *right S*-valine methyl ester salt

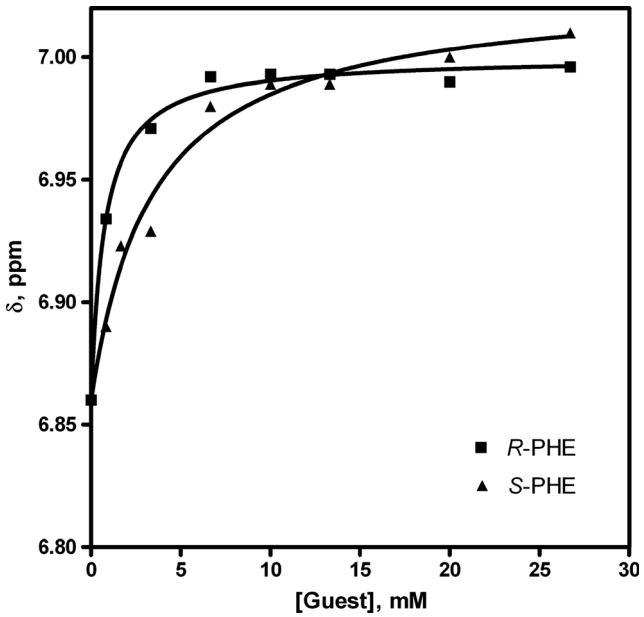

Fig. 3 Non-linear dependence on the concentration of the enantiomers of valine ester salts fitted to Eq. 4 of ^{1}H NMR chemical shifts of the methyl groups of isopropyl in receptor **5**

former group constitutes the dynamic part of the molecule. Potential energy changes and the RMSD obtained for the receptor compared to its lowest energy conformation as a function of time during the MD is presented in the Supplementary Material (Fig. S1). RMSD changes show that the major conformational fluctuation occurs in the *N*-benzyl group, caused by rotation around the N–C bond. The conformer with higher population (Fig. 5a) was used to accommodate ligands as described in the Computational methods. All the complexes were computed for MD calculations over a period of 20 ns at 300 K as described above. Potential energy changes and RMSD compared to the lowest energy conformer as a function of time during the MD for each complex are presented in the Supplementary Material (Fig. S1). These indicate that MD calculations produced good results over the 20-ns period. Although the ligands were placed on the surface of the crown ring bearing the isopropyl group where ligands are allowed to interact with isopropyl group, the MD calculations highlight that the isopropyl group is flipped over so that the ligand is sandwiched between the benzyl site arm and the benzene unit in the crown ring. These two groups form a pseudo-chiral binding site for ED where enantiomers are sandwiched between these two rings, hence the isopropyl group is not involved in recognition or, consequently, in the discrimination process. The conformers of the complexes of the receptor with the enantiomers possessing the highest populations obtained from MD calculations are illustrated in Fig. 5b–d. They demonstrate that the receptor holds the ligands on the surface of the crown cavity via hydrogen bonds. Nevertheless, in the case of the receptor complex with the methyl ester of the alanine salt, the benzyl group provides an interaction site for the ammonium group through cation-π interactions [85–93], probably due to its smaller site compared with benzyl in phenylalanine and isopropyl in valine.

Table 1 Experimental binding constants calculated by ^{1}H NMR titration and enantiomeric discrimination (ED) properties of receptor **5** for amino acid ester and organoammonium salts at 300 K

Ligand	$K_d \times 10^3$, M [a]	K_a, M^{-1} [b]	K_a^R/K_a^S [c]	ED [d]	EDF [e]
R-ALA	1.13±0.43	885	1.85	65 R	30
S-ALA	2.09±0.27	478			
R-PHE	0.72±0.13	1,389	4.93	83.1 R	66.2
S-PHE	3.54±0.92	282			
R-VAL	2.52±0.37	397	0.26	79.4 S	58.8
S-VAL	0.660±0.087	1,515			

[a] Dissociation constants calculated by non-linear curve fitting of dependency of chemical shifts on the concentration of ligands

[b] Association constants calculated by $K_a = 1/K_d$

[c] Ratio of the binding constants for each enantiomer

[d] ED calculated from K_a^R/K_a^S and assuming R+S =100

[e] ED factor calculated by the difference in ED for each enantiomer (ED_R - ED_S)

The reason for the slightly better recognition of the *R*-alanine salt by the receptor may be attributed to the fact that its methyl site arm adopts a preferable orientation for interaction with the benzyl group, and the CH group of the methyl site arm also has a good contact point with the benzene ring (Fig. 5b). As for the complexes of the receptor with the two enantiomers of phenylalanine, a similar mode of action with that of alanine is observed, with the phenyl group sandwiched periplanarly between the two aromatic groups of the receptor by interacting via π–π contacts. Thus, this is the most likely explanation for why these enantiomers are largely discriminated by the receptor. Unlike alanine and phenylalanine, the *S* enantiomer of valine is preferably bound by the receptor. This implies that the isopropyl group of valine has an unfavorable interaction with the benzyl group of the receptor, and instead has a favorable interaction with the benzene unit of the crown ring as mentioned earlier.

Contact point analysis

Contact point analyses (intermolecular bond distances) were performed to observe the dynamic changes in the ligands complexed to the receptor during MD trajectories recorded for 20 ns. Bond distances were selected between the HA (the hydrogen attached to the stereogenic carbon of alanine) and hetero atoms in the receptor. The changes in distance during this period between HA and N1, O1, O2, O3, and O4 for *R*-alanine salt are presented in Supplementary Material (Fig. S2). Average values of 4.753±0.220, 3.214±0.375,

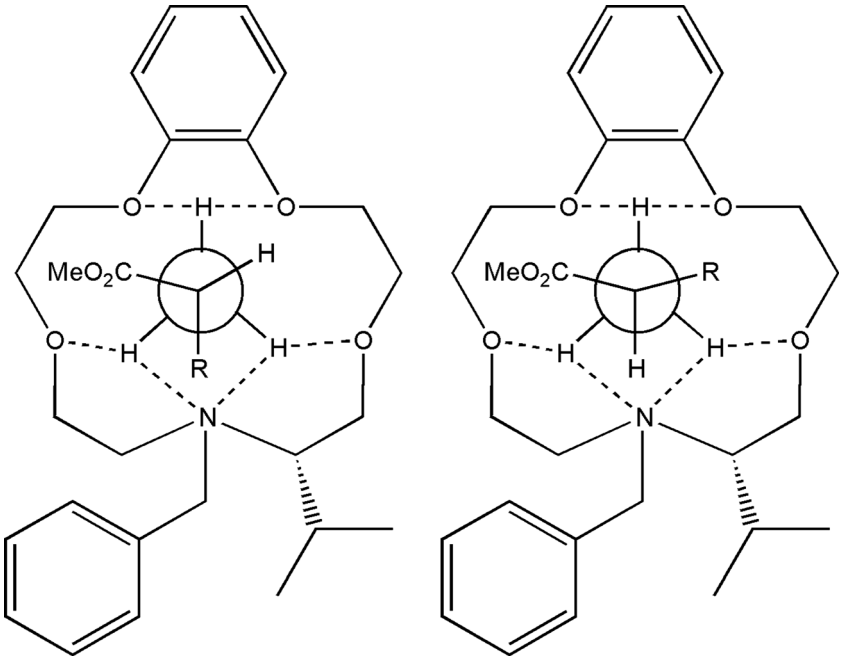

Fig. 4 A possible representative interaction of receptor **5** with *R* (*left*) and *S* (*right*) enantiomers of amino acid ester salts

4.459±0.219, 3.317±0.427 and 2.249±0.248 Å, respectively, were found. The hydrogen bond analysis for one of ammonium hydrogens of the ligand with N1 in the receptor was also investigated and an average value of 2.795±0.248 Å was found for this bond. The results indicate that HA has rather a close contact with O4 and that, during the MD calculations, this atom spends a large fraction of time facing towards the benzene ring. This is expected since the conformer with the highest population demonstrates that HA orients towards the benzene ring.

MM-PBSA method

The binding free energies (kcal mol^{-1}) of the host to guests estimated by MM-PBSA are shown in Table 2. The values are quite large compared with experimental results. This may be

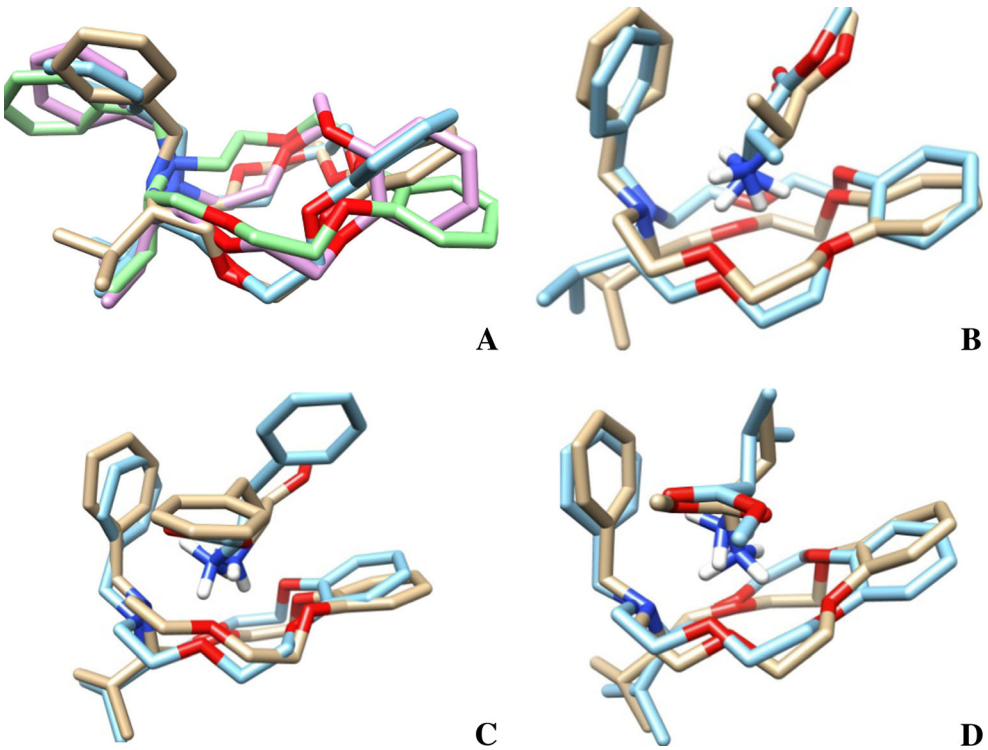

Fig. 5 **a** Structures corresponding to the four lowest conformers of receptor **5** obtained from cluster analysis of trajectories from molecular dynamic (MD) simulations. Out of 300 clusters: *brown* 127 clusters, *blue* 18 clusters, purple and green 9 clusters. **b**–**d** The superimposed lowest energy conformers of the complexes of enantiomers of alanine (**b**), phenylalanine (**c**), valine (**d**) obtained from the cluster analysis of MD trajectories. *Brown R* enantiomers, *blue S* enantiomers

Table 2 Binding energies calculated by experimental (^{1}H NMR) and theoretical (MM-PBSA) methods for complexes of receptor **5** with ligands

Ligand	ΔG_{exp} [a]	$\Delta\Delta G_{exp}$ [b]	$-\Delta E_{PB}$ [c]	$\Delta\Delta E_{PB}$ [d]	$-T\Delta S$ [e]	$-\Delta G_{PB}$ [f]	$\Delta\Delta G_{PB}$ [g]
R-ALA	−4.02	−0.36	13.42±1.70	−0.3	12.81±1.11	0.61	−0.14
S-ALA	−3.66		13.72±1.73		13.25±1.80	0.47	
R-PHE	−4.29	−1.58	17.21±1.86	−1.45	14.29±1.38	2.92	−0.59
S-PHE	−3.34		15.76±2.12		13.43±1.33	2.33	
R-VAL	−3.54	0.80	40.47±2.84	0.88	13.63±1.40	26.84	1.55
S-VAL	−4.34		41.35±2.21		12.96±1.12	28.39	

[a] Experimentally observed binding free energies (in kcal mol^{-1}) between the receptor and the ligands obtained from $\Delta G_{exp}=-RT\ln K_a$ taken from Table 1

[b] The difference between the experimental determined binding free energies (in kcal mol^{-1}) for each enantiomer

[c] The estimated binding free energies (in kcal mol^{-1}) using both Poisson-Boltzmann solvation model for each enantiomer

[d] The difference between the calculated binding energies (in kcal mol^{-1}) for each enantiomer

[e] Entropy changes ($T\Delta S$, in kcal mol^{-1}) upon complexation calculated by nmode analyses

[f] The difference in the calculated binding free energies by MM-PBSA (in kcal mol^{-1}) for each enantiomer

[g] The difference between the calculated binding free energies (in kcal mol^{-1}) for each enantiomer

attributed to the fact that the guest molecules are charged and the MM-PBSA method utilizes the continuum solvation model, where solute–solvent interactions are ignored. Therefore, it is expected that this method will overestimate the binding free energies of such systems. However, it is interesting to note that the estimated binding free energies calculated by MM-PBSA are quite close to experimental values. This difference may be attributed to the solvation energy since the MD calculations are performed in implicit solvation.

Negative entropy values derived from NMODE calculations were obtained for all complexes, meaning that the conformational freedom of ligand and receptor were reduced upon complexation. This is expected since it is generally acknowledged that there is entropy loss upon binding, due mainly to the translation entropy loss of receptor and ligand, although some compensation is gained from the disorder of the solvation of the solute (the ligand) and the release of bonded solvent from the receptor to the bulk. This effect cannot be calculated explicitly since the continuum solvation models represent the solvent as a continuous medium instead of individual "explicit" solvent molecules, and do not include any bonding interactions.

Density functional theory

The computational description of noncovalent interactions between biomolecules that are important in the maintenance of the 3D structures of DNA, RNA, and proteins [94–98] is essential for the design and development of drug molecules [99]. The CCSD(T) [coupled cluster with singles and doubles including perturbative triples] method is the current standard for accurately estimating the interaction energy of noncovalently bound complexes in small systems [100]. Nonetheless, the formal O ($N7$) complexity of the method hampers its applicability. Computationally less expensive methods are required to describe such interactions in larger systems. Approximate DFT is another current option for investigating a variety of chemical systems involving dozens of atoms or more [101]. Nevertheless, the method is limited by the failure of most density functional approximations to describe dispersion interactions, which can be essential in noncovalent complexes. These interactions intrinsically involve long-range electron correlation effects, which are not

Table 3 Energies calculated for each enantiomer by DFT (B3LYP and M06-2X) methods using 6–31+G(d) basis sets. The values within parenthesis involve calculations at the same levels in chloroform with the polarizable continuum model (PCM)

Ligands	E (B3LYP) [a]	ΔE [b]	E (M06-2X) [c]	ΔE [d]
R-ALA	−1,653.5449914	−1.17	−1,652.8457826	−0.42
	(−1,653.5905668)	(−1.53)	(−1,652.8924410)	(−4.48)
S-ALA	−1,653.5431215		−1,652.8451179	
	(−1,653.5881256)		(−1,652.8852865)	
R-PHE	−1,884.6001296	−0.84	−1,883.8102166	−0.54
	(−1,884.6447669)	(−0.27)	(−1,883.8574072)	(−2.15)
S-PHE	−1,884.59878640		−1,883.8093548	
	(−1,884.6443320)		(−1,883. 8539815)	
R-VAL	−1,732.16960837	−0.74	−1,731.43892611	−1.66
	(−1,732.21407490)	(−0.52)	(−1,731.4831505)	(−2.00)
S-VAL	−1,732.16843283		−1,731.43628008	
	(−1,732.21325120)		(−1,731.4799606)	

[a] The total energy of the complexes calculated by B3LYP/6-31+G(d) in Hartree

[b] The difference between the calculated total energy of each enantiomer (in kcal mol^{-1}) by B3LYP/6-31+G(d)

[c] The total energy of the complexes calculated by (M062X/6-31+G(d) in Hartree

[d] The difference between the calculated total energy of each enantiomer (in kcal mol^{-1}) by M062X/6-31+G(d)

captured by the popular local or semilocal density functionals [102–108]. Several approaches have been taken to improve the density functionals currently used to handle dispersion effects [109–119]. Alternatively, for noncovalent interactions, Zhao and Truhlar have launched highly parametrized empirical M05-2X and M06-2X functionals with a good deal of promise [80–83]. These functionals implicitly account for medium-range electron correlations because they are parametrized in this respect, which is satisfactory to express the dispersion interactions within many complexes [88] but they have still to be fully developed for noncovalent interactions of biological relevance. Lorenzo and Grana have recently reported stacking and hydrogen bond interactions between adenine and gallic acid calculated by DFT and DFT-SAPT [120].

The present study employed two DFT methods (B3LYP and M06-2X) using the same basis set, 6-31+g(d), in the investigation of noncovalent interactions for the molecular complexes of the receptor with amino acid ester salts. These functionals estimated the noncovalent interactions, composed mainly of hydrogen bonds, involved in these molecular complexes, which could establish a model for biological systems. The two methods produced different results despite a similar trend with the experimental data. Nevertheless, B3LYP seemed to perform better compared to M062X (Table 3). Complexes of the receptor with phenylalanine enantiomers were calculated by B3LYP using 6-31+g(3d) basis sets. The energies obtained for *R* and *S* enantiomers were −1, 884.67950885 and −1,884.67818497 Hartrees, respectively. This corresponds to a difference of −0.88 kcal mol^{-1}, compared with −0.84 kcal mol^{-1} found for the difference calculated using 6-31+g(d) basis sets. It appears that the calculations in chloroform with PCM make no significant contribution to the energy difference between the complexes of the receptor with enantiomer pairs (Table 3).

Overestimation of the binding free energies for the complexes by QM calculations might be associated with poor handling of intermediate and long-range correlation and dispersion. Proper handling of hydrogen bonding using DFT remains a concern. Sherrill [121] has reported a careful benchmark study using the potential energy curves for six dimer combinations involving formic acid, formamide, and formamidine.

Conclusions

Molecular recognition by synthetic models is of great practical interest in many applications such as chemical detection, separation and encapsulation, and enantioselective synthesis. These simplified models may be relevant for biological molecular recognition since the same physical principles are involved in both processes. Therefore, modeling studies often produce delicate and usually unpredictable results. These may be used to further a detailed understanding of biomolecular interactions, which is very difficult to achieve in living cells. However, despite significant advances in molecular modeling techniques and the relative simplicity of model systems, development of a tractable and theoretically sound computational method is still required to interpret experimental data, which will finally be helpful for the design of new model hosts for targeted molecular guests.

The current work represents an experimental (^{1}H NMR titration) and theoretical study of the molecular recognition of the molecular complexes of chiral aza-15-crown-5 ether with methyl esters of amino acid salts in order to understand the mode of binding and the main forces driving ED. The results obtained from NMR titration reveal that the receptor binds enantiomers with moderate binding constants, with phenylalanine being more largely discriminated with a difference of −1.58 kcal mol^{-1} in binding free energy. The differences in the theoretical binding energies were also calculated by MM-PBSA and DFT [B3LYP/6-31+G(d) and M06-2X/6-31+G(d)]. The data obtained give valuable information regarding the molecular recognition mode of the organoammonium complexes of chiral aza-crown ether with C_1 symmetry, which may be relevant to biological systems.

Acknowledgments We are grateful to Dicle University Research Council for financial support (DUAPK-02-FF-20, DUBAP-05-FF-31 and DUBAP-05-FF-32), Dr. Selami Ercan for Gaussian 09 facilities, The Scientific and Technological Research Council of Turkey (TÜBİTAK) for TR-GRID facilities and Professor D. Case for a waiver license of AMBER.

References

1. Barron LD (1986) True and false chirality and absolute asymmetric synthesis. J Am Chem Soc 108:5539
2. Quack M (2002) How important is parity violation for molecular and biomolecular chirality? Angew Chem Int Ed 41:4618
3. Knowles WS (2002) Asymmetric hydrogenations (Nobel Lecture). Angew Chem Int Ed 41:1998
4. Noyori R (2002) Asymmetric catalysis: science and opportunities (Nobel Lecture). Angew Chem Int Ed 41:2008
5. Sharpless KB (2002) Searching for new reactivity (Nobel Lecture). Angew Chem Int Ed 41:2024
6. Cram JD (1998) The design of molecular hosts, guests, and their complexes (Nobel Lecture). Angew Chem Int Ed 27:1009
7. Pedersen CJ (1998) The discovery of crown ethers (Noble Lecture). Angew Chem Int Ed Engl 27:1021
8. Lehn JM (1998) Supramolecular chemistry-scope and perspectives molecules, supermolecules, and molecular devices (Nobel Lecture). Angew Chem Int Ed Engl 27:87
9. Atwood JL, Davies J, MackNikol, DD (1996) In: Vögtle F (ed) Elsevier, Oxford, pp 1–10
10. Lehn JM (1995) Supramolecular chemistry. VCH, Weinheim
11. Pedersen CJ (1967) Cyclic polyethers and their complexes with metal salts. J Am Chem Soc 89:7017–7036
12. Lehn JM, Sirlin C (1978) Molecular catalysis: enhanced rates of thiolysis with high structural and chiral recognition in complexes

of a reactive macrocyclic receptor molecule. J Chem Soc Chem Commun 949–951
13. Stoddart JF (1979) From carbohydrates to enzyme analogues (Tate and Lyle Lecture). Chem Soc Rev 8:85–142
14. Chadwick DJ, Cliffe A, Stutther IO (1981) Chiral diaza −18-crown −6-derivatives. J Chem Soc Chem Commun 19:992–994
15. Mizutani T, Ema T, Tomita T, Kuroda Y, Ogoshi H (1994) Design and synthesis of a trifunktional chiral porphyrin with C-2 symmetry as a chiral recognition host for amino -acid esters. J Am Chem Soc 116:4240–4250
16. Kyba EB, Koga K, Sousa LR, Siegel MG, Cram DJ (1973) Chiral recognition in molecular complexing. J Am Chem Soc 95: 2692–2693
17. Stoddart JF (1988) Chiral crown ethers. In: Eliel EL, Wilen SH (eds) Topics in stereochemistry, vol 17. Wiley, New York, pp 207–288
18. Zhang XX, Bradshaw JS, Izatt RM (1997) Enantiomeric recognition of amine compounds by chiral macrocyclic receptors. Chem Rev 97:3313–3361
19. Behr JP, Lehn JM, Vierling P (1976) Stable ammonium cryptates of chiral macrocyclic receptor molecules bearing amino-acid side-chains. J Chem Soc Chem Commun 1976:621–623
20. Cram DJ, Cram JM (1978) Design of complexes between synthetic hosts and organic guests. Acc Chem Res 11:8–14
21. Kyba EP, Timko JM, Kaplan LJ, De Jong F, Gokel GW, Cram DJ (1978) Host-guest complexation. 11. Survay of chiral recognition of amine and amino ester salts by bilocular bidinaphthyl hosts. J Am Chem Soc 100:4555–4568
22. Lingenfelter DS, Helgeson RC, Cram DJ (1981) Host-guest complexation 23. High chiral recognition of amino-acid and ester guests by hosts containing one chiral element. J Org Chem 46:393–406
23. Davidson RB, Bradshaw JS, Jones BA, Dalley NK, Christensen JJ, Izatt RM, Morin FG, Grant DM (1984) Enantiomeric recognition of organic ammonium-salts by chiral crown ethers based on the pyridino-18-crown-6 structure. J Org Chem 49:353–357
25. Iimori T, Erickson SD, Rheingold AL, Still WC (1989) Enantioselective complexation with a conformationally homogeneous C_2 podand ionophore. Tetrahedron Lett 30:6947–6950
26. Maruyama K, Sohmiya H, Tsukube H (1989) New chiral host molecules derived from naturally occurring monensin ionophore. J Chem Soc Chem Commun 864–865
27. Bradshaw JS, Huszthy P, McDaniel CW, Zhu CY, Dalley NK, Izatt RM, Lifson S (1990) Enantiomeric recognition of organic ammonium salts by chiral dialkyl-, dialkenyl- and tetramethyl-substituted pyridino-18-crown-6 and tetramethyl-subsituted bis-pyridino-18-crown-6 ligands: comparison of the temperature dependent ^{1}H NMR and empirical force field techniques. J Org Chem 55: 3129–3137
28. Huszthy P, Bradshaw JS, Zhu CY, Izatt RM, Lifson S (1991) Recognition by new symmetrıcally substituted chiral diphenylbutylpyridino-18-crown-6 and di-tert-butylpyridino-18-crown-6 and asymmetrically substituted chiral dimethylpyridıno-18-crown-6 ligands of the enantiomers of various organic ammonium perchlorates. J Org Chem 56:3330–3336
29. Li G, Still WC (1991) Podand sulfones-enantioselective receptors for peptidic ammonium-ions. J Org Chem 56:6964–6966
30. Wang X, Erickson SD, Iimori T, Still WC (1992) Enantioselective complexation of organic ammonium-ions by simple tetracyclic podand ionophores. J Am Chem Soc 114:4128–4137
31. Armstrong A, Still WC (1992) Enantioselective cation binding with a functionalized podand ionophore. J Org Chem 57:4580–4582
32. Miyake H, Yamashita T, Kojima Y, Tsukube H (1995) Enantioselective transport of amino-acid ester salts by macrocyclic pseudopeptides containing n, n-ethylene-bridged-dipeptide units. Tetrahedron Lett 36:7669–7672
33. Araki K, Inada K, Shinkai S (1996) Chiral recognition of alpha-amino acid derivatives with a homooxacalix[3]arene: construction of a pseudo-C-2-symmetrical compound from a C-3-symmetrical macrocycle. Angew Chem Int Ed Engl 35:72–74 Angew Chem 108:92–94
34. Gerczei T, Bocskei Z, Keseru GM, Samu E, Huszthy P (1999) Enantiomeric recognition of alpha-(1-naphthyl)ethylammonium perchlorate by enantiomerically pure dimethylphenazino-18-crown-6 ligand in solid and gas phases. Tetrahedron Asymmetry 10:1995–2005
35. Turgut Y, Sahin E, Togrul M, Hosgoren H (2004) The enantiomeric recognition of chiral organic ammonium salts by chiral monoaza-15-crown-5 ether derivatives. Tetrahedron Asymmetry 15: 1583–1588
36. Kim J-K, Song S, Kim J, Kim TH, Kim H, Suh H (2006) Synthesis of chiral azophenolic pyridino-18-crown-6 ether and its enantiomeric recognition toward chiral primary amines. Bull Kor Chem Soc 27:1577–1580
37. Karakaplan M, Turgut Y, Aral T, Hosgoren H (2006) The synthesis and formation of complexes between derivatives of chiral Aza-18-crown-6 ethers and chiral primary organic ammonium salts. J Incl Phenom Macrocycl Chem 54:315–319
38. Karakaplan M, Ak D, Colak M, Kocakaya OS, Hosgoren H, Pirinccioglu N (2013) Synthesis of new diaza-18-crown-6 ethers derived from trans-(R, R)-1,2-diaminocyclohexane and investigation of their enantiomeric discrimination ability with amino acid ester salts. Tetrahedron 69:349–358
39. Yilmaz T, Hosgoren H (2003) Synthesis of chiral monoaza-15-crown-5 ethers from L-valinol and the enantiomeric recognition of chiral amines and their perchlorates salts. Tetrahedron Asymmetry 14:3815–3818
40. El-Barghouthi MI, Jaime C, Akielah RE, Al-Sakhen NA, Masoud NA, Issa AA, Badwanand AA, Zughul MB (2009) Free energy perturbation and MM/PBSA studies on inclusion complexes of some structurally related compounds with beta-cyclodextrin. Supramol Chem 21:603–610
41. El-Barghouthi MI, Jaime C, Al-Sakhen NA, Issa AA, Abdoh AA, Al Omari MM, Badwan AA, Zughul MB (2008) Molecular dynamics simulations and MM-PBSA calculations of the cyclodextrin inclusion complexes with 1-alkanols, para-substituted phenols and substituted imidazoles. J Mol Struct (THEOCHEM) 853:45–52
42. Choi Y, Jung S (2004) Molecular dynamics (MD) simulations for the prediction of chiral discrimination of N-acetylphenylalanine enantiomers by cyclomaltoheptaose (beta-cyclodextrin, beta-CD) based on the MM-PBSA (molecular mechanics-Poisson-Boltzmann surface area) approach. Carbohydr Res 339:1961–1966
43. Nunez-Aguero C-J, Escobar-Llanos C-M, Diaz D, Jaimec C, Garduno-Juarez R (2006) Chiral discrimination of ibuprofen isomers in β-cyclodextrin inclusion complexes: experimental (NMR) and theoretical (MD, MM/GBSA) studies. Tetrahedron 62: 4162–4172
44. Srinavasan J, Cheatham TE, Cieplak P, Kollman PA, Case DA (1998) Continuum solvent studies of the stability of DNA, RNA and phosphoramidate-DNA helices. J Am Chem Soc 120:9401–9409
45. Gouda H, Kuntz ID, Case DA, Kollman PA (2003) Free energy calculations for theophylline binding to an RNA aptamer: comparison of MM-PBSA and thermodynamic integration methods. Biopolymers 68:16–34
46. Trieb M, Rauch C, Wibowo FR, Wellenzohn B, Leidl KB (2004) Cooperative effects on the formation of intercalationsites. Nucleic Acids Res 32:4696–4703
47. Fogolari F, Tosatto SCE (2005) Application of MM/PBSA colony free energy to loop decoy discrimination: toward correlation between energy and root mean square deviation. Protein Sci 14:889–901
48. Gohlke H, Case DA (2004) Converging free energy estimates: MM-PB(GB)SA studies on the protein-protein complex Ras-Raf. J Comput Chem 25:238–250

49. Kuhn B, Gerber P, Schulz-Gasch T, Stahl M (2005) Validation and use of the MM-PBSA approach for drug discovery. J Med Chem 48: 4040–4048
50. Kuhn B, Kollman PA (2000) Binding of a diverse set of ligands to avidin and streptavidin: an accurate quantitative prediction of their relative affinities by a combination of molecular mechanics and continuum solvent models. J Med Chem 43:3786–3791
51. Lee MR, Duan Y, Kollman PA (2000) Use of MM-PB/SA in estimating the free energies of proteins: application to native, intermediates, and unfolded villin headpiece. Proteins Struct Funct Genet 39:309–316
52. Wang J, Morin P, Wang W, Kollman PA (2001) Use of MM-PBSA in reproducing the binding free energies to HIV-1 RT of TIBO derivatives and predicting the binding mode to HIV-1 RT of efavirenz by docking and MM-PBSA. J Am Chem Soc 123: 5221–5230
53. Wang W, Kollman PA (2000) Free energy calculations on dimer stability of the HIV protease using molecular dynamics and a continuum solvent model. J Mol Biol 303:567–587
54. Pearlman DA (2005) Evaluating the molecular mechanics Poisson-Boltzmann surface area free energy method using a congeneric series of ligands to p38 MAP kinase. J Med Chem 48:7796–7807
55. Lyne PD, Lamb ML, Saeh JC (2006) Accurate prediction of the relative potencies of members of a series of kinase inhibitors using molecular docking and MM-GBSA scoring. J Med Chem 49: 4805–4808
56. Weis A, Katebzadeh K, Soderhjelm P, Nilsson I, Ryde U (2006) Ligand affinities predicted with the MM/PBSA method: dependence on the simulation method and the force field. J Med Chem 49:6596–6606
57. Fielding L (2000) Determination of association constants (K-a) from solution NMR data. Tetrahedron 56:6151–6170
58. Hirose KA (2001) practical guide for the determination of binding constants. J Inc Phenom Macrocycl Chem 39:193–209
59. Case DA, Darden TA, Cheatham TE III, Simmerling CL, Wang J, Duke RE, Luo R, Merz KM, Pearlman DA, Crowley M, Walker RC, Zhang W, Wang B, Hayik S, Roitberg A, Seabra G, Wong KF, Paesani F, Wu X, Brozell S, Tsui V, Gohlke H, Yang L, Tan C, Mongan J, Hornak V, Cui G, Beroza P, Mathews DH, Schafmeister C, Ross WS, Kollman PA (2006) AMBER 9. University of California, San Francisco
60. Frisch MJ, Trucks GW, Schlegel HB, Scuseria GE, Robb MA, Cheeseman JR, Montgomery Jr JA, Vreven T, Kudin KN, Burant JC, Millam JM, Iyengar SS, Tomasi J, Barone V, Mennucci B, Cossi M, Scalmani G, Rega N, Petersson GA, Nakatsuji H, Hada M, Ehara M, Toyota K, Fukuda R, Hasegawa J, Ishida M, Nakajima T, Honda Y, Kitao O, Nakai H, Klene M, Li X, Knox JE Hratchian HP, Cross JB, Bakken V, Adamo C, Jaramillo J, Gomperts R, Stratmann RE, Yazyev O, Austin AJ, Cammi R, Pomelli C, Ochterski JW, Ayala PY, Morokuma K, Voth GA, Salvador P, Dannenberg JJ, Zakrzewski VG, Dapprich S, Daniels AD, Strain MC, Farkas O, Malick DK, Rabuck AD, Raghavachari K, Foresman JB, Ortiz JV, Cui Q, Baboul AG, Clifford S, Cioslowski J, Stefanov BB, Liu G, Liashenko A, Piskorz P, Komaromi I, Martin R L, Fox DJ, Keith T, Al-Laham MA, Peng CY, Nanayakkara A, Challacombe M, Gill PMW, Johnson B, Chen W, Wong MW Gonzalez C, Pople JA (2004) Gaussian 03, Revision C.02, Gaussian, Inc., Wallingford CT
61. Dewar MJS, Zoebisch EG, Healy EF, Stewart JJP (1985) Development and use of quantum mechanical molecular models. 76. AM1: a new general purpose quantum mechanical molecular model. J Am Chem Soc 107:3902–3909
62. Jakalian A, Bush BL, Jack DB, Bayly CI (2000) Fast, efficient generation of high-quality atomic charges. AM1-BCC model: I. Method. J Comput Chem 21:132–14
63. Jakalian A, Jack DB, Bayly CI (2002) Fast, efficient generation of high-quality atomic charges. AM1-BCC model: II. Parameterization and validation. J Comput Chem 23:1623–1641
64. Hornak V, Abel R, Okur A, Strockbine B, Roitberg A, Simmerling C (2006) Comparison of multiple Amber force fields and development of improved protein backbone parameters. Proteins 65: 712–725
65. Wang J, Wolf RM, Caldwell JW, Kollman PA, Case DA (2004) Development and testing of a general amber force field. J Comput Chem 25:1157–1174
66. Pettersen EF, Goddard TD, Huang CC, Couch GS, Greenblatt DM, Meng EC, Ferin TE (2004) UCSF chimera—a visualization system for exploratory research and analysis. J Comput Chem 25: 1605–1612
67. Kollman PA, Massova I, Reyes C, Kuhn B, Huo S, Chong L, Lee M, Lee T, Duan Y, Wang W, DoniniO O, Cieplak P, Srinivasan J, Case DA, Cheatham TE (2000) Calculating structures and free energies of complex molecules: combining molecular mechanics and continuum models. Acc Chem Res 33:889–897
68. Srinivasan J, Cheatham TE, Cieplak P, Kollman PA, Case DA (1998) Continuum solvent studies of the stability of DNA, RNA, and hosphoramidate-DNA helices. J Am Chem Soc 120: 9401–9409
69. Cornell WD, Cieplak CI, Bayly IR, Gould IR, Merz KM, Ferguson DM, Spellmeyer DC, Fox T, Caldwell JW, Kollman PA (1995) A second generation force field for the simulation of proteins, nucleic acids, and organic molecules. J Am Chem Soc 117:5179–5197
70. Cramer CJ, Truhlar DG (1999) Implicit solvation models: equilibria, structure, spectra and dynamics. Chem Rev 99:2161–2200
71. Simonson T (2003) Electrostatics and dynamics of proteins. Rep Prog Phys 66:737–787
72. Still WC, Tempczyk A, Hawley R, Hendrickson T (1990) Semianalytical treatment of solvation for molecular mechanics and dynamics. J Am Chem Soc 112:6127–6129
73. McQuarrie DA (1976) Statistical mechanics. Harper & Row, New York
74. Brooks BR, Janezic D, Karplus M (1995) Harmonic analysis of large systems. J Comput Chem 16:1522–1553
75. Stewart JJP (2007) Optimization of parameters for semiempirical methods. V: modification of NDDO approximations and application to 70 elements. J Mol Model 13:1173–1213
76. Becke AD (1993) Density-functional thermochemistry 3. The role of exact exchange. J Chem Phys 98:5648–5652
77. Lee C, Yang W, Parr RG (1988) Development of the colle-salvetti correlation-energy formula into a functional of the electron-density. Phys Rev B 37:785–789
78. Vosko SH, Wilk L, Nusair M (1980) Accurate spin-dependent electron liquid correlation energies for local spin-density calculations-a critical analysis. Can J Phys 58:1200–1211
79. Stephens PJ, Devlin FJ, Chabalowski CF, Frisch MJ (1994) Ab-intio calculation of vibrational absorption and circular-dichroism spectra using density-functional force-fields. J Phys Chem 98: 11623–11627
80. Zhao Y, Schultz NE, Truhlar DG (2005) Exchange-correlation functional with broad accuracy for metallic and nonmetallic compounds, kinetics, and noncovalent interactions. J Chem Phys 123:161103
81. Zhao Y, Schultz NE, Truhlar DG (2006) Design of density functionals by combining the method of constraint satisfaction with parametrization for thermochemistry, thermochemical kinetics, and noncovalent interactions. J Chem Theory Comput 2:364–382
82. Zhao Y, Truhlar DG (2006) A new local density functional for main-group thermochemistry, transition metal bonding, thermochemical kinetics, and noncovalent interactions. J Chem Phys 125:194101
83. Zhao Y, Truhlar DG (2008) The M06 suite of density functionals for main group thermochemistry, thermochemical kinetics, noncovalent interactions, excited states, and transition elements: two new

functionals and systematic testing of four M06-class functionals and 12 other functionals. Theor Chem Accounts 120:215–241
84. Frisch MJ, Trucks GW, Schlegel HB, Scuseria GE, Robb MA, Cheeseman JR, Scalmani G, Barone V, Mennucci B, Petersson GA, Nakatsuji H, Caricato M, Li X, Hratchian HP, Izmaylov AF, Bloino J, Zheng G, Sonnenberg JL, Hada M, Ehara M, Toyota K, Fukuda R, Hasegawa J, Ishida M, Nakajima T, Honda Y, Kitao O, Nakai H, Vreven T, Montgomery Jr JA, Peralta JE, Ogliaro F, Bearpark M, Heyd JJ, Brothers E, Kudin KN, Staroverov VN, Kobayashi R, Normand J, Raghavachari K, Rendell A, Burant JC, Iyengar SS, Tomasi J, Cossi M, Rega N, Millam JM, Klene M, Knox JE, Cross JB, Bakken V, Adamo C, Jaramillo J; Gomperts R, Stratmann RE, Yazyev O, Austin AJ, Cammi R, Pomelli C, Ochterski JW, Martin RL, Morokuma K, Zakrzewski VG, Voth GA, Salvador P, Dannenberg JJ, Dapprich S, Daniels AD, Farkas Ö, Foresman JB, Ortiz JV, Cioslowski J, Fox DJ (2009) Gaussian 09, Revision A.1, Gaussian, Inc., Wallingford CT
85. Umezawa NY, Hirota M, Taceuchi Y (1995) The CH/pi interaction-significance in molecular recognition. Tetrahedron 51:8665–8701
86. Olson CA, Shi Z, Kallenbach NR (2001) Polar interactions with aromatic side chains in alpha-helical peptides: CH center dot center dot center dot O H-bonding and cation-pi interactions. J Am Chem Soc 123:6451–6452
87. Shi Z, Olson CA, Kallenbach NR (2002) Cation-pi interaction in model alpha-helical peptides. J Am Chem Soc 124:3284–3291
88. Orner BP, Salvatella X, Quesada JS, de Mendoza J, Giralt E, Hamilton AD (2002) De novo protein surface design: use of cation-pi interactions to enhance binding between an alpha-helical peptide and a cationic molecule in 50 % aqueous solution. Angew Chem Int Ed 41:117–119
89. Pletneva EV, Laederach AT, Fulton DB, Kostic NM (2001) The role of cation-pi interactions in biomolecular association. Design of peptides favoring interactions between cationic and aromatic amino acid side chains. J Am Chem Soc 123:6232–6245
90. Burghardt TP, Juranic N, Macura S, Ajtai K (2002) Cation-pi interaction in a folded polypeptide. Biopolymers 63:261–272
91. Fernandez-Recio J, Vazquez A, Civera C, Sevilla P, Sancho J (1997) The tryptophan/histidine interaction in alpha-helices. J Mol Biol 267:184–197
92. Tsou LK, Tatko CD, Waters ML (2002) Simple cation-pi interaction between a phenyl ring and a protonated amine stabilizes an alpha-helix in water. J Am Chem Soc 124:14917–14921
93. Malone JF, Murray CM, Charlton MH, Docherty R, Lavery AJ (1997) X-H center dot center dot center dot pi(phenyl) interactions—theoretical and crystallographic observations. J Chem Soc Faraday Trans 93:3429–3436
94. Saenger W (1984) Principles of nucleic acid structure. Springer, New York
95. Shieh HS, Berman HM, Dabrow M, Neidle S (1980) The structure of drug-deoxydinucleoside phosphate complex; generalized conformational behavior of intercalation complexes with RNA and DNA fragments. Nucleic Acids Res 8:85–97
96. Elstner M, Hobza P, Frauenheim T, Suhai S, Kaxiras E (2001) Hydrogen bonding and stacking interactions of nucleic acid base pairs: a density-functional-theory based treatment. J Chem Phys 114:5149–5155
97. Meyer EA, Castellano RK, Diederich F (2003) Interactions with aromatic rings in chemical and biological recognition. Angew Chem Int Ed Engl 42:1210–1250
98. Burley SK, Petsko GA (1985) Aromatic-aromatic interaction: a mechanism of protein structure stabilization. Science 229:23–28
99. Mobley DL, Graves AP, Chodera JD, McReynolds AC, Shoichet BK, Dill KA (2007) Predicting absolute ligand binding free energies to a simple model site. J Mol Biol 371:1118–1134
100. Raghavachari K, Trucks GW, Pople JA, Head-Gordon M (1989) Fifth-order perturbation comparison of electron correlation theories. Chem Phys Lett 157:479–483
101. Parr RG, Yang W (1989) Density-functional theory of atoms and molecules, vol 16. International series of monographs on chemistry. Oxford University Press, New York
102. Tsuzuki S, Luthi HP (2001) Interaction energies of van der Waals and hydrogen bonded systems calculated using density functional theory: assessing the PW91 model. J Chem Phys 114:3949–3957
103. Cerny J, Hobza P (2005) The X3LYP extended density functional accurately describes H-bonding but fails completely for stacking. Phys Chem Chem Phys 7:1624–1626
104. Allen MJ, Tozer DJ (2002) Helium dimer dispersion forces and correlation potentials in density functional theory. J Chem Phys 117:11113–11120
105. Hobza P, Sponer J, Reschel T (1995) Density functional theory and molecular clusters. J Comput Chem 16:1315–1325
106. Kristyan S, Pulay P (1994) Can (semi)local density functional theory account for the London dispersion forces? Chem Phys Lett 229:175–180
107. Kurita N, Sekino H (2003) Ab initio and DFT studies for accurate description of van der Waals interaction between rare-gas atoms. Int J Quantum Chem 91:355–362
108. Johnson ER, Wolkow RA, DiLabio GA (2004) Application of 25 density functionals to dispersion-bound homomolecular dimers. Chem Phys Lett 394:334–338
109. von Lilienfeld OA, Tavernelli I, Rothlisberger U, Sebastiani D (2004) Optimization of effective atom centered potentials for London dispersion forces in density functional theory. Phys Rev Lett 93:153004
110. von Lilienfeld OA, Tavernelli I, Rothlisberger U, Sebastiani D (2005) Performance of optimized atom-centered potentials for weakly bonded systems using density functional theory. Phys Rev B 71:195119
111. Dion M, Rydberg H, Schroder E, Langreth DC, Lundqvist BI (2004) Van der Waals density functional for general geometries. Phys Rev Lett 92:246401
112. Becke AD, Johnson ER (2005) A density-functional model of the dispersion interaction. J Chem Phys 123:154101
113. Johnson ER, Becke AD (2005) A post-Hartree–Fock model of intermolecular interactions. J Chem Phys 123:024101
114. Becke AD, Johnson ER (2006) Exchange-hole dipole moment and the dispersion interaction: high-order dispersion coefficients. J Chem Phys 124:014104
115. Zimmerli U, Parrinello M, Koumoutsakos P (2004) Dispersion corrections to density functionals for water aromatic interactions. J Chem Phys 120:2693–2699
116. Jurecka P, Cerny J, Hobza P, Salahub DR (2007) Density functional theory augmented with an empirical dispersion term. Interaction energies and geometries of 80 noncovalent complexes compared with ab initio quantum mechanics calculations. J Comput Chem 28:555–569
117. Wu Q, Yang W (2002) Empirical correction to density functional theory for van der Waals interactions. J Chem Phys 116:515–524
118. Grimme S (2006) Semiempirical GGA-type density functional constructed with a long-range dispersion correction. J Comput Chem 27:1787–1799
119. Grimme S (2004) Accurate description of van der Waals complexes by density functional theory including empirical corrections. J Comput Chem 25:1463–1473
120. Lorenzo I, Grana AM (2013) Stacking and hydrogen bond interactions between adenine and gallic acid. J Mol Model 19:5293–5299
121. Thanthiriwatte KS, Hohenstein EG, Burns LA, Sherrill CD (2011) Assessment of the performance of DFT and DFT-D methods for describing distance dependence of hydrogen-bonded interactions. J Chem Theory Comput 7:88–96